Wind stress forcing of the Oregon coastal ocean during the 1999 upwelling season

R. Samelson, P. Barbour, J. Barth, S. Bielli, T. Boyd, D. Chelton, P. Kosro, M. Levine, and E. Skyllingstad

College of Oceanic and Atmospheric Sciences, Oregon State University, Corvallis, Oregon, USA

J. Wilczak

Environmental Technology Laboratory, NOAA, Boulder, Colorado, USA

Received 3 April 2001; revised 1 October 2001; accepted 6 November 2001; published 1 May 2002.

[1] The wind stress forcing of the Oregon coastal ocean during June–August 1999 is estimated from a regional mesoscale atmospheric model and from satellite scatterometer observations, supplemented by moored and coastal surface data and by a land-based wind profiler. Both the mean and variable components of model alongshore wind stress increase by factors of 3–4 from north to south along the Oregon coast. There is evidence of orographic intensification near Cape Blanco, which is supported by previous aircraft and ship observations during August 1995. The systematic southward increase of southward stress will drive enhanced ocean upwelling along the southern Oregon coast and suggests the new hypothesis that systematic variations in local wind stress may contribute to the observed offshore displacement of the coastal upwelling jet in this region. It is inferred from an analysis of the model and surface data that ocean upwelling modifies coastal surface air temperatures by 1–5°C over timescales of 12–24 hours. *INDEX TERMS:* 3329 Meteorology and Atmospheric Dynamics: Mesoscale meteorology; 3339 Meteorology and Atmospheric Dynamics: Ocean/atmosphere interactions (0312, 4504); 4219 Oceanography: General: Continental shelf processes; 4279 Oceanography: General: Upwelling and convergences; *KEYWORDS:* coastal upwelling, coastal meteorology, air-sea coupling, marine atmospheric boundary layer, mesoscale modeling, remote sensing

1. Introduction

[2] It is well known that wind stress is the primary driving mechanism for upwelling circulations along much of the U.S. west coast, including the Oregon coastal ocean, and in many other coastal regions [e.g., *Allen*, 1980]. Consequently, characterizing and understanding coastal wind fields is an important component of the study of coastal ocean circulation. Many oceanographically relevant aspects of meteorological variability along the U.S. west coast have been identified, ranging from the statistical properties of large-scale atmospheric forcing [*Halliwell and Allen*, 1987] to the local properties of the atmospheric boundary layer [*Beardsley et al.*, 1987]. Many of these studies were carried out during the 1981–1982 Coastal Ocean Dynamics Experiment off the coast of northern California. However, with a few exceptions involving aircraft measurements during limited time periods, estimates of wind stress in the Oregon coastal zone have been based on sparse buoy measurements, primarily concentrated along the central portion of the coast, and have contained little or no information on spatial variability of the wind stress field.

[3] Along the central Oregon coast during summer, a southward oceanic jet develops in response to wind-driven ocean upwelling. Recent studies have established that this jet often separates from the coast near Cape Blanco, along the southern Oregon coast, and moves offshore. This marks the northernmost point where the California Current broadens offshore to develop the intense, meandering, equatorward flow regime that dominates the physical variability of the eastern boundary region west of California [*Barth et al.*, 2000; *Barth and Smith*, 1998]. In addition to its influence on regional physical characteristics, this offshore displacement of the jet provides an important mechanism for cross-shelf exchange of chemical and biological materials. The dynamics of the separation process are not currently understood. Previous studies have proposed [*Barth et al.*, 2000; *Barth and Smith*, 1998] and explored [*Dale and Barth*, 2001] the hypothesis that the separation arises when the upwelling jet encounters topographic features along the shelf and slope near Cape Blanco.

[4] The results reported here suggest an alternative hypothesis: The separation of the upwelling jet from the coast may arise in response to persistently strong local winds near and south of Cape Blanco. More generally, our results demonstrate the presence of systematic spatial variations in both the mean and time-varying components of wind stress in the Oregon coastal zone during the summer 1999 upwelling season, with important implications for the coastal ocean response. These results are based primarily on simulations conducted with a regional mesoscale atmospheric model and on satellite scatterometer observations. The simulations were conducted as part of an intensive oceanographic observational and modeling program conducted during summer 1999 in the Oregon coastal zone, with support from the National Oceanographic Partnership Program (NOPP).

[5] Our main purpose here is to summarize new estimates of coastal wind stress fields that have significant implications for the study of ocean circulation dynamics in the coastal zone. A comprehensive comparison of model results with scatterometer and surface observations, over a much longer time period than considered here, is in progress and will be reported on elsewhere. The present results are relevant to continuing observational and modeling studies of coastal circulation that will focus on the Oregon coastal zone in 2001 and in following years. The assumption of spatially uniform wind-stress forcing has recently been

0148-0227/02/2001JC000900$09.00

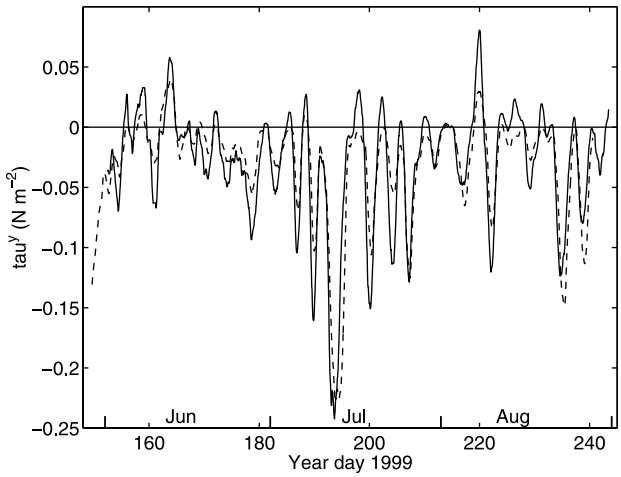

Figure 1. NDBC-46050 (solid line) and Advanced Regional Prediction System (ARPS) (dashed line) alongshore wind stress versus year day 1999. Both series are 25-hour running means of hourly values. Hourly buoy stress was computed from 1-hour average buoy winds, assuming neutral stability. Hourly model stress was computed from instantaneous model stress by interpolating linearly to the buoy location.

identified as a leading source of model error in data-assimilating model studies of Oregon coastal ocean circulation [*Oke et al.*, 2002]. The present contribution serves also to document estimated wind stress fields that are being used in extensions of these recent modeling studies. In addition, a brief comparison of offshore buoy and land-based coastal meteorological observations is presented that is relevant to the use of land-based data to estimate forcing fields over the coastal ocean.

2. Methods

2.1. Regional Atmospheric Model

[6] Regional atmospheric simulations were conducted at Oregon State University (OSU) on a regular basis during summer 1999 using the University of Oklahoma Advanced Regional Prediction System (ARPS) mesoscale model [*Xue et al.*, 1995]. ARPS is a nonhydrostatic model with explicit microphysics, a terrain-following vertical coordinate, and a nested grid capability. Our implementation of the ARPS model used a $60 \times 60 \times 32$ *xyz* Lambert-conformal grid, with an outer 36-km nest and an inner 12-km nest, both centered on 44.7°N 124°W (Newport, Oregon), and vertical grid increment increasing from 20 m near the surface to 450 m at altitude. The 12-km domain extended offshore past 128°W, and roughly from 42°N to 47°N meridionally (see Figures 2 and 8c below). The model was run in a forecast mode, with 36-hour forecasts computed daily from 0000 UTC. The simulations were initialized with 0000 UTC 40-km analyses from the National Center for Environmental Prediction (NCEP) Eta model [*Black*, 1994], and time-dependent boundary conditions on the outer nest were obtained from the corresponding Eta forecasts. The outer and inner nest simulations were computed sequentially, with the boundary conditions on the inner nest obtained from the outer nest simulation. Surface fluxes over the ocean are computed by a bulk formulation, with stability corrections based on the model surface air temperature and on an imposed sea surface temperature (SST) field, which is here taken from the NCEP Eta SST analysis.

[7] For the present analysis a 92-day time series of model wind stress was constructed using hours 4–27 of each simulation during 29 May through 28 August 1999 (year days 149–240), referred to here as "June–August." Archiving of model results was begun on 29 May, and 0000 UTC NCEP analyses were not available for 29–30 August, so we have truncated the series at 28 August. The 0000 UTC NCEP analyses were not available for an additional three isolated days during June–August. We have used hours 28–36 from the previous day's simulation and simulations initialized from 1200 UTC analyses for these 3 days to complete the time series. Since the central Oregon coast is aligned roughly along a meridian, we refer to the zonal and meridional components of wind as "cross-shore" and "alongshore," respectively. For the analysis of the wind stress field, these components have been obtained by appropriately transforming the horizontal model velocities from the Lambert-conformal grid, which results in a small but measurable rotation near the edges of the domain. This geometric adjustment is negligible near the center of the domain and was not applied for the comparisons with observations discussed in section 3.5.

2.2. Satellite Scatterometer

[8] Data from the SeaWinds scatterometer onboard the QuikSCAT satellite were obtained for the period from 21 July (day 202), the start date of the QuikSCAT data record, through 28 August 1999. The SeaWinds scatterometer is a scanning microwave radar that infers the wind stress from measurements of radar backscatter from the roughness of the sea surface at multiple antenna look angles [*Naderi et al.*, 1991]. In terms of the equivalent neutral stability wind at 10 m, the accuracy of scatterometer wind retrievals has been estimated to be $\sim$1 m s^{-1} in speed and $\sim$20° in direction [*Freilich and Dunbar*, 1999].

[9] The QuikSCAT orbit provides twice-daily coverage of the Oregon coastal zone, nominally at 0300 and 1400 UTC (2000 and 0700 PST). The resolution of individual QuikSCAT estimates of vector stress is 25 km. Rain-contaminated observations were flagged and eliminated by comparison with independent satellite measurements of rain rate within 50 km and 1 hour. The resulting scatterometer stress fields were individually examined to remove observations that contained evidence of noise from unflagged rain events or from other sources. This procedure yielded 53 scatterometer stress fields during the July–August period of interest. Some additional uncertainties are associated with the stress values immediately adjacent to the coast, so these should be interpreted with caution. No attempt was made to remove diurnal effects from the scatterometer stress fields.

2.3. Buoy and Land-Based Observations

[10] Surface meteorological observations were obtained from the National Oceanic and Atmospheric Administration (NOAA) buoy NDBC-46050 (44.62°N 124.53°W), an OSU meteorological buoy (44.64°N, 124.32°W), and a land-based NOAA surface meteorological (CMAN) station at Newport (44.61°N, 124.07°W). A 915-MHz Radio Acoustic Sounding System (RASS) profiler at the same Newport site provided wind and equivalent potential temperature observations from near the surface to roughly 1500 m. The OSU meteorological buoy and the RASS profiler were deployed with support from the OSU NOPP project. The OSU buoy was located roughly 20 km from the coast, halfway between the coast and NDBC-46050.

[11] The NDBC-46050 and OSU buoy winds were corrected to 10 m from 5 and 2.9 m, respectively, assuming neutral stability. The Newport CMAN anemometer height was 9.4 m, so no correction was necessary. The NDBC-46050 and Newport CMAN stations are roughly continuous during June–August 1999, but have intermittent missing values. The OSU buoy wind, pressure, and temperature records are continuous until 20 July, 9 August, and 6 August (days 201, 221, and 218), respectively, when they end due to instrument failures. The wind stress for NDBC-46050 and for the OSU buoy were computed from 1-hour averaged winds, using the *Large and Pond* [1981] bulk flux formulation with neutral stability. Neutral stability was assumed in these

calculations because SST observations sufficient to allow computation of stability corrections were available only for the incomplete record at the OSU buoy and because inhomogeneities in the coastal zone SST field introduce additional uncertainty in the stability corrections. At the OSU buoy the difference of observed air and 2-m ocean temperatures during June through 6 August had mean value −0.04°C and standard deviation 1.22°C, so the assumption of neutral stability is reasonable, especially during the periods of strong winds that are of particular interest here. Stability effects could alter the bulk stresses by 10–30%, or perhaps more, during limited periods when air-sea temperature differences were larger or when winds were weak.

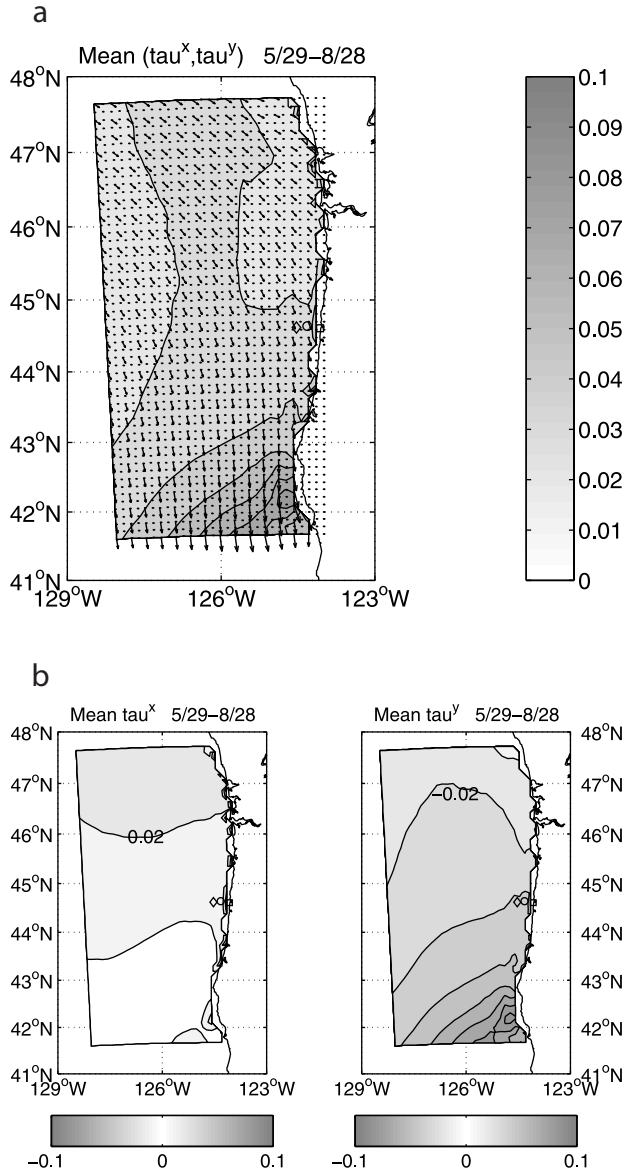

Figure 2. (a) Vector and (b) cross-shore (left panel) and alongshore (right panel) ARPS mean wind stress for June–August 1999. In Figure 2a, vectors are overlaid on contours of total stress, and are shown only at every second model grid point; the full model grid over the western half of the 12-km domain is indicated by dots. Contour interval is 0.01 N m^{-2}. In Figure 2b the labeled contours are 0.02 N m^{-2} for cross-shore stress and −0.02 N m^{-2} for alongshore stress. Locations of NDBC-46050 (diamond) and OSU (circle) buoys and Newport CMAN/RASS (square) sites are indicated.

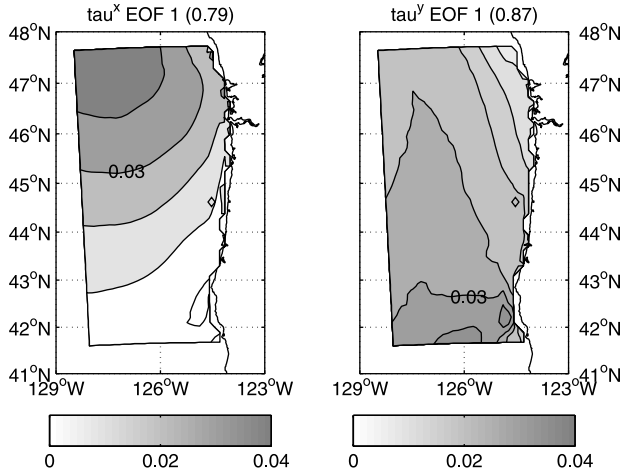

Figure 3. First empirical orthogonal functions (EOFs) of (left) cross-shore and (right) alongshore ARPS wind stress fluctuations for June–August 1999. Contour intervals are 0.01 (left) and 0.005 (right). Labeled contours are 0.03 in both panels. Products of these EOFs and amplitudes in Figure 4 give stress in N m^{-2}.

3. Results

3.1. Wind Stress at NDBC-46050

[12] During June–August 1999, there were roughly 7–10 dominant upwelling-favorable (southward) wind stress events along the Oregon coast, as indicated by time series of 25-hour running mean wind stress estimated from buoy NDBC-46050 wind observations and from the atmospheric model (Figure 1). These events have typical amplitudes of 0.1 N m^{-2} and timescales of 1–2 days. The strongest event occurred on 12–14 July (days 193–195), with mean southward stress exceeding 0.2 N m^{-2}.

[13] Overall, the interpolated model stress represents the observed stress well at the buoy NDBC-46050 location, supporting

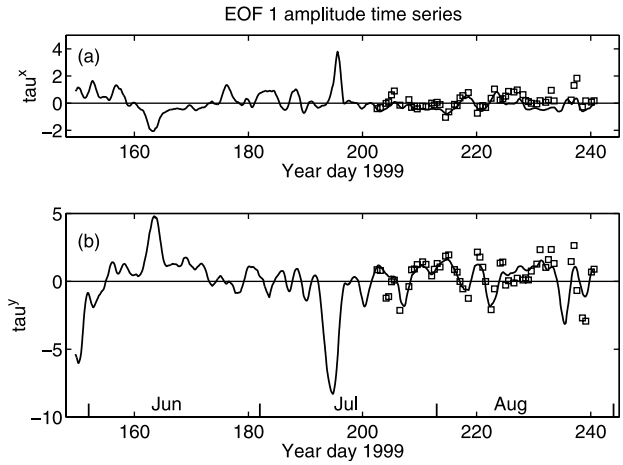

Figure 4. Amplitude time series for first EOFs of (a) alongshore and (b) cross-shore ARPS wind stress fluctuations versus year day 1999. Although the alongshore and cross-shore EOFs were computed separately, these two time series are correlated with each other, with correlation coefficient −0.58. Amplitude time series for the first EOFs of alongshore (Figure 4a) and cross-shore (Figure 4b) scatterometer stress fluctuations are also shown (squares). Products of these amplitudes and EOFs in Figures 3 and 6 give stress in N m^{-2}.

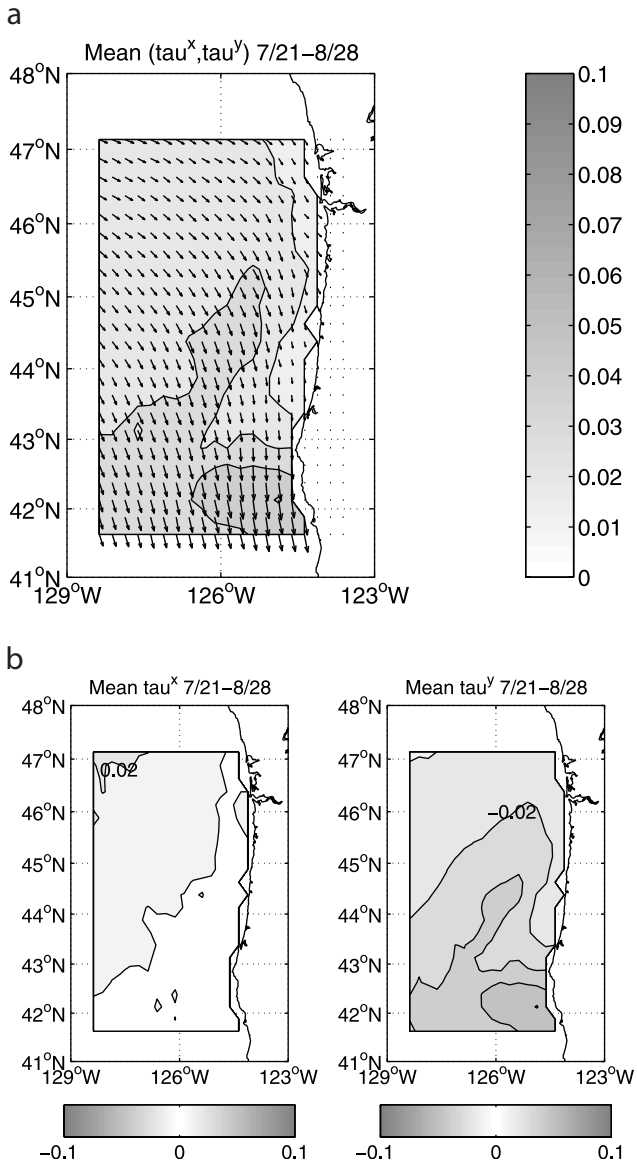

Figure 5. (a) Vector and (b) cross-shore (left panel) and alongshore (right panel) scatterometer mean wind stress for 21 July through 28 August 1999. Contour interval is 0.01 N m^{-2}. Values immediately adjacent to the coast have additional uncertainty and should be interpreted with caution.

the hypothesis that the model results presented in section 3.2 are useful estimates of the coastal zone wind stress fields. All of the significant stress events in the buoy series are also seen in the model series. The model stress estimate is sometimes substantially smaller than the buoy stress, and there are two events in late August in which the model stress is larger than the buoy stress. The largest stress event (days 193–195) lasts half a day longer in the model series than in the buoy series; this and several other events also occur several hours later in the model series than in the buoy series.

3.2. Model Wind Stress Fields

[14] The mean model wind stress fields for June–August 1999 are shown in Figure 2. The mean stress increases southward along the coast and rotates from southeastward in the north to southward in the south. The mean alongshore stress increases southward along the coast by a factor of >4, from 0.02 N m^{-2} in the north to >0.08 N m^{-2} just south of Cape Blanco. The mean cross-shore stress decreases southward from 0.025 N m^{-2} in the north to <0.01 N m^{-2} in the south. Most of the southward intensification of southward stress occurs over the southern third of the domain, between 44°N and 42°N.

[15] The first empirical orthogonal functions (EOFs) of cross-shore and alongshore stress fluctuations and the associated amplitude time series from the model fields are shown in Figures 3 and 4. The means were removed from both series prior to the EOF computation. The variability in cross-shore stress decreases southward and toward the coast, while that in alongshore stress increases southward and is largest in the vicinity of Cape Blanco. Since the alongshore stress is of primary interest for coastal ocean circulation modeling, the EOFs were computed separately for the cross-shore and alongshore stress. The running 25-hour mean model stress time series for June–August 1999 were used for this computation. The first EOFs of alongshore and cross-shore stress explain 87% and 79%, respectively, of the variance in the corresponding stress fields. Consequently, the respective amplitude time series (Figure 3) closely follow the stress time series at most locations, including the NDBC-46050 buoy (Figure 1). The EOF calculation was repeated for July–August 1999, in order to verify that the strong southward stress event in early June (days 150–155; see Figure 1) did not control the spatial structure of the EOFs; the resulting EOFs were very similar to those in Figure 3.

3.3. Scatterometer Wind Stress Fields

[16] The mean wind stress fields in the Oregon coastal region from the 53 overpasses of the QuikSCAT scatterometer during 21 July through 28 August 1999 (days 202–240) are shown in Figure 5. The mean alongshore stress is southward and increases in magnitude southward along the coast by a factor of 3, from <0.02 N m^{-2} in the north to >0.05 N m^{-2} just south of Cape Blanco. The mean cross-shore stress decreases southward from 0.02 N m^{-2} in the north to <0.01 N m^{-2} along the coast in the south.

[17] The first EOFs of cross-shore and alongshore stress fluctuations, and the associated amplitude time series from the scatterometer stress fields, are shown in Figures 6 and 4. These EOFs explain 64% and 62% of the variance in the stress fields. As represented by these first EOFs, the variability in cross-shore stress decreases southward and toward the coast, while that in alongshore stress increases southward and is largest in the vicinity of Cape Blanco.

[18] Since the model and scatterometer means and EOFs in Figures 2–6 were computed for different periods, they cannot be

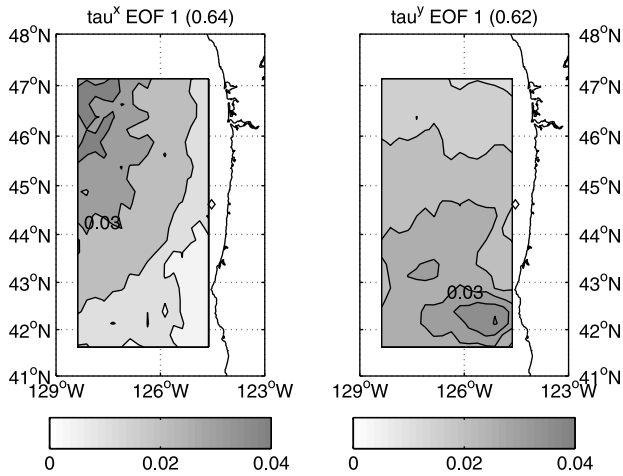

Figure 6. First EOFs of cross-shore (left) and alongshore (right) scatterometer wind stress for 21 July through 28 August 1999. Contour intervals are 0.01 (left panel) and 0.005 (right panel). Values immediately adjacent to the coast have additional uncertainty and should be interpreted with caution. Products of these EOFs and amplitudes in Figure 4 give stress in N m^{-2}.

Table 1. Statistics of Hourly Observed Surface Cross-Shore (u) and Alongshore (v) Winds, Pressure (p), and Air Temperature (T) for NDBC-46050 and OSU Meteorological Buoys and Newport CMAN Station During Common Data Periods for June–August 1999[a]

		NDBC-46050		OSU Buoy				
	N	Mean	Std	Mean	Std	Corr	Bias	RMSE
u	1091	1.9	2.3	1.3	1.9	0.78	−0.6	1.6
v	1091	−2.8	4.6	−2.3	4.2	0.94	0.5	1.6
p	1549	1018.0	3.0	1018.6	3.0	1.00	0.6	0.6
T	1494	13.4	1.4	12.8	1.5	0.86	−0.7	1.0
		NDBC-46050		Newport CMAN				
	N	Mean	Std	Mean	Std	Corr	Bias	RMSE
u	2067	1.3	2.0	0.9	1.5	0.30	−0.3	2.1
v	2067	−2.6	4.5	−1.2	3.9	0.78	1.3	3.1
p	2075	1017.8	3.1	1018.2	3.1	0.99	0.5	0.6
T	2085	13.9	1.5	12.7	1.8	0.76	−1.1	1.6
		OSU Buoy		Newport CMAN				
	N	Mean	Std	Mean	Std	Corr	Bias	RMSE
u	1199	1.3	1.8	0.9	1.7	0.48	−0.4	1.8
v	1199	−2.2	4.2	−1.2	3.9	0.82	1.0	2.6
p	1664	1018.6	3.0	1018.6	3.0	1.00	−0.1	0.3
T	1591	12.7	1.5	12.2	1.7	0.81	−0.6	1.2

[a] NDBC buoy and CMAN statistics are for 1 June through 31 August 1999. OSU buoy statistics are for 1 June through 20 July (u, v), 9 August (p), and 6 August (T). Winds are given in m s^{-1}, pressure is given in millibars, and air temperature is given in °C. N, number of points; Std, standard deviation; Corr, correlation between time-series at each pair of sites; Bias, second site mean minus first site mean; RMSE, root-mean-square difference.

directly compared. A more rigorous comparison of the model and scatterometer fields during a much longer, coincident time period is in progress and will be reported on elsewhere. Note also that no attempt has been made to correct the scatterometer means or EOFs for possible biases due to diurnal or other effects. Nonetheless, despite the differing temporal coverage, the scatterometer and model fields have strong qualitative similarities. In both, the mean and variable components of alongshore stress increase, and those of cross-shore stress decrease, toward the south. In both, the variable components of alongshore stress have a minimum along the central Oregon coast, and mean and variable alongshore stress is locally intensified near Cape Blanco. This is an additional indication that the dominant spatial structures found here are persistent features of the coastal wind stress field.

[19] There are also interesting and important differences between the scatterometer and model fields. For example, the scatterometer shows a pronounced minimum in mean alongshore stress adjacent to the central Oregon coast and a systematic offshore increase in cross-shore stress (Figure 5); neither of these features appear in the model estimates (Figure 2). It is possible that this difference may be related to the combined effect of errors in model SST (see section 4.2) and to the dependence of stress on boundary

Table 2. Statistics of Hourly Observed and Model Surface Cross-Shore (u) and Alongshore (v) Winds, Pressure (p), and Air Temperature (T) for NDBC-46050 and OSU Meteorological Buoys and Newport CMAN Station and for Model Variables at Corresponding Locations[a]

		NDBC-46050		Model				
	N	Mean	Std	Mean	Std	Corr	Bias	RMSE
u	2010	1.3	2.0	1.9	1.8	0.52	0.6	2.0
v	2010	−2.6	4.5	−3.2	3.8	0.81	−0.6	2.7
p	2018	1017.7	3.1	1017.3	3.2	0.93	−0.4	1.2
T	2029	13.9	1.5	14.5	2.0	0.65	0.6	1.7
		OSU Buoy		Model				
	N	Mean	Std	Mean	Std	Corr	Bias	RMSE
u	1281	1.2	1.8	2.1	1.9	0.57	0.8	1.9
v	1281	−2.5	4.2	−3.0	4.1	0.80	−0.6	2.7
p	1750	1018.9	3.1	1017.9	3.1	0.92	−1.0	1.6
T	1676	12.6	1.5	13.6	1.9	0.40	1.0	2.1
		Newport CMAN		Model				
	N	Mean	Std	Mean	Std	Corr	Bias	RMSE
u	2031	0.8	1.4	1.5	1.7	0.61	0.7	1.5
v	2031	−1.2	3.9	−1.8	2.6	0.75	−0.6	2.6
p	2031	1018.4	3.1	1013.9	3.2	0.94	−4.5	4.6
T	2031	12.7	1.8	14.4	3.0	0.56	1.7	3.0

[a] NDBC buoy and CMAN statistics are for 1 June through 31 August 1999. OSU buoy statistics are for 1 June through 20 July (u, v), 9 August (p), and 6 August (T). Winds are given in m s^{-1}, pressure is given in millibars, and air temperature is given in °C. N, number of points; Std, standard deviation; Corr, correlation between time-series at each pair of sites; Bias, second site mean minus first site mean; RMSE, root-mean-square difference.

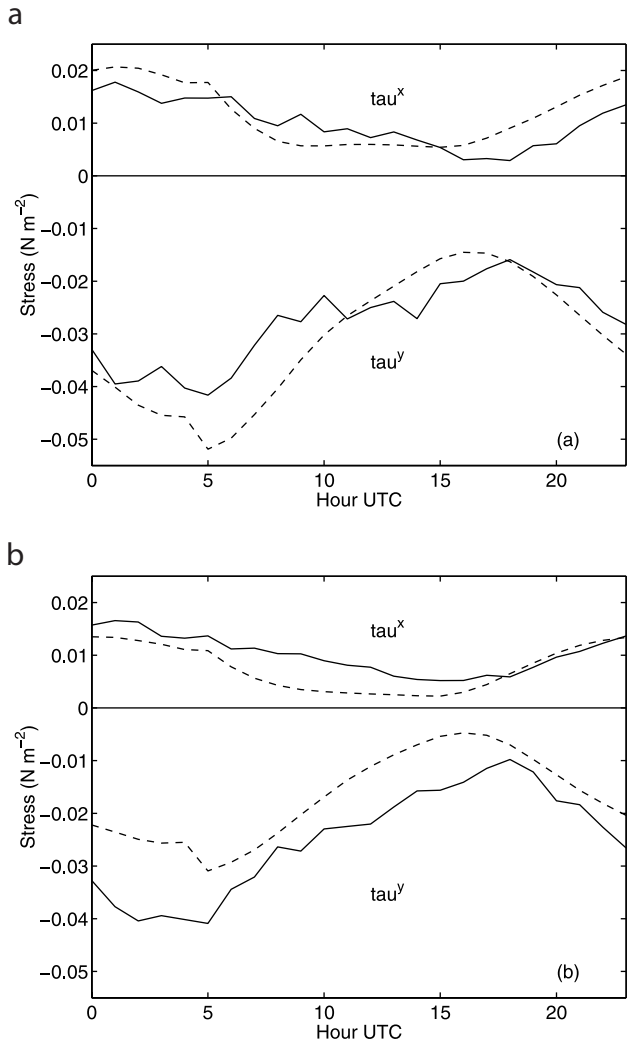

Figure 7. (a) NDBC-46050 (solid line) and ARPS (dashed line) mean diurnal cycle of cross-shore (positive, eastward) and alongshore (negative, southward) wind stress during 29 May through 28 August 1999. (b) As in Figure 7a, but for Oregon State University (OSU) buoy (solid line) and ARPS (dashed line) for 29 May through 20 July 1999.

layer stability. As noted above, the scatterometer stress values immediately adjacent to the coast have additional uncertainties and must therefore be viewed with caution. Further analysis of these differences is in progress and will be reported on elsewhere.

3.4. Surface Observations

[20] The statistics of NDBC-46050 and OSU buoy and Newport CMAN meteorological observations during June–August 1999 are presented in Table 1 (see Figure 2 for locations of these observations). The mean alongshore winds are southward, 2.5–3 m s^{-1} at the buoys and 1.2 m s^{-1} at the Newport CMAN station. During the common data periods the mean alongshore wind is 0.5 m s^{-1} weaker at the OSU buoy than at NDBC-46050 and an additional 1 m s^{-1} weaker at the Newport CMAN station (Table 1). The diurnal offshore motion of the low-level alongshore jet [e.g., *Bielli et al.*, 2002; *Burk and Thompson*, 1996] probably contributes to the onshore decrease of mean alongshore wind over the water. Frictional and orographic effects presumably intensify this decrease over land toward the CMAN station. The mean cross-shore winds are eastward, roughly 1.5 m s^{-1} at the buoys and 1 m s^{-1} at the Newport CMAN station.

[21] Statistical comparisons of surface and model variables during June–August 1999 are presented in Table 2. These comparisons generally support the assumption that the model simulations are accurate enough to provide quantitative information on the spatial structure of the wind field, especially for the alongshore component of stress, consistent with the general agreement between the model and scatterometer stress fields discussed in sections 3.2 and 3.3. For all three surface stations the correlations between modeled and observed pressure, and between modeled and observed alongshore wind, are high. In contrast, the model-observation correlations for cross-shore wind and surface air temperature are relatively low (Table 2). The mean wind biases are all <1 m s^{-1} and are less than the magnitudes of the respective mean winds. The large differences in mean pressures at the Newport CMAN station are due primarily to uncorrected model and observation-site topographic height differences, associated with local topography that is not resolved in the model. In all cases, the model and observed standard deviations are comparable, the largest differences being for alongshore wind and temperature at the Newport CMAN station (Table 2). The root-mean-square differences between the model and observed alongshore wind and pressure time series are less than the corresponding standard deviations at both buoys, and the same is true for alongshore wind at the Newport CMAN station. The mean surface air temperatures are 1–2°C warmer in the model than the observations; as discussed in section 5, this is probably due primarily to the influence of SST variations associated with coastal upwelling that are not resolved by the NCEP SST analysis used in the model ocean surface boundary conditions. As described in section 2.3, the stress estimates from the meteorological observations do not include stability corrections, so we have chosen to make this statistical comparison in terms of winds instead of stress, consistent with the usual practice for meteorological model verification.

3.5. Diurnal Cycle at NDBC-46050

[22] The mean diurnal cycles of stress from the hourly model and buoy stress time series are shown in Figure 7. These cycles were computed by averaging the stress at each hour of the day during June–August 1999 for NDBC 46050 and during June through 20 July for the OSU buoy. The overall mean stress has not been removed. This period spans the summer solstice, so aliasing of the cycle from changes in local length of day is minimal. The maximum southward mean buoy stress is 0.04 N m^{-2} and is reached during late afternoon and evening (hours 0000–0400 UTC, 1700–2100 PST). The minimum southward buoy stress is 0.02 N m^{-2} at NDBC-46050 and 0.01 N m^{-2} at the OSU buoy and is reached during midmorning (1700 UTC, 1000 PST). The mean and variable diurnal eastward buoy stresses are much weaker, with a cycle amplitude of roughly 0.01 N m^{-2}, a maximum near 0000 UTC, and a minimum near 1600 UTC.

[23] The model diurnal cycle generally resembles the observed cycle at each buoy, but appears to weaken onshore more rapidly than the observed cycle. The model southward stress maximum is 0.05 N m^{-2} and occurs a few hours later than the buoy stress maxima; the model southward stress minimum is roughly 0.005 N m^{-2} and occurs 2 hours earlier than the buoy stress minima. The mean and variable diurnal eastward model stress is broadly similar to the eastward stress at both buoys, with the model stress minimum occurring nearly 8 hours earlier and persisting for 5–6 hours longer than the buoy stress minima. Note that the scatterometer overpass times are nominally 0300 and 1400 UTC, coincidentally close to the extreme phases of the diurnal cycle.

3.6. Wind Profiler Observations

[24] We have compared the hourly mean diurnal cycles and the overall means, standard deviations, and correlations of Newport RASS profiler and model winds in the lower atmosphere for June–August 1999. We report more completely on this comparison elsewhere [*Bielli et al.*, 2002]. Generally, the results again support

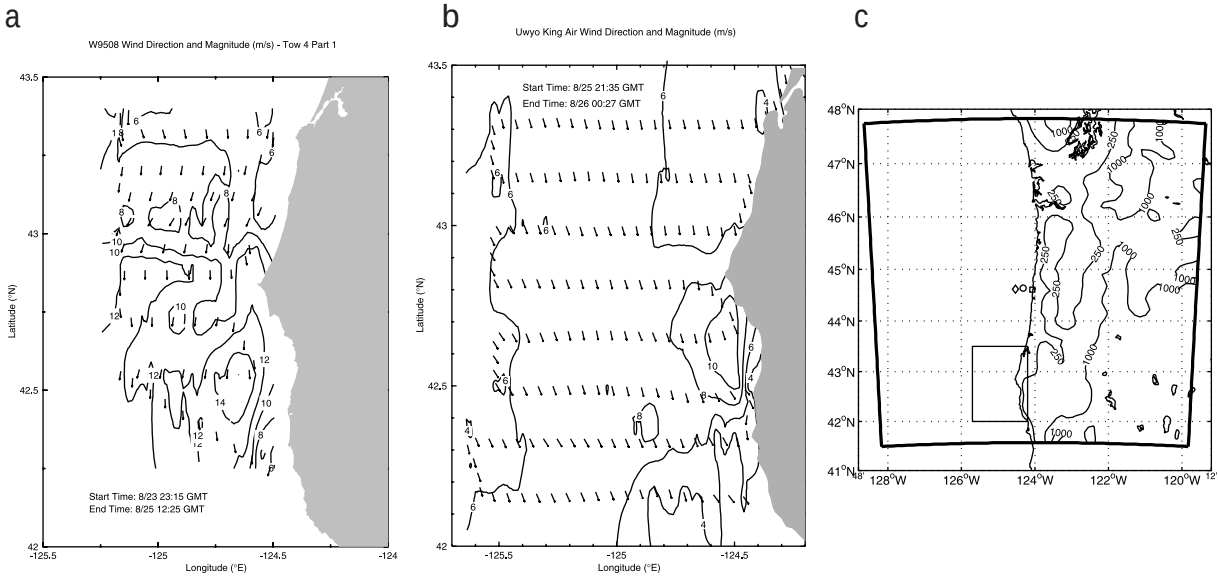

Figure 8. In situ observations of surface winds near Cape Blanco (August 1995). (a) Wind speed contours (m s^{-1}) and wind direction (arrows) from R/V *Wecoma* observations near Cape Blanco (42.7°N, 124.6°W) on a 36-hour cruise track during 23–25 August 1995. (b) Wind speed contours (m s^{-1}) and wind direction (arrows) at 30 m from University of Wyoming King Air observations near Cape Blanco on a 3-hour flight track during 25–26 August 1995. The intensified southward winds near 42.5°N, 124.7°W in these observations are similar to features in the 1999 model results (Figures 5 and 6) and are presumably the result of orographic intensification associated with supercritical flow around Cape Blanco. (c) Region of ship and aircraft observations from Figures 8a and 8b (small box) relative to 12-km atmospheric model domain (large box) and model topography (250 and 1000 m contours).

the conclusion that the model performed sufficiently well that it should provide useful estimates of the wind field. The timing and depth of the model diurnal cycle agree roughly with the observations. Model and profiler means and standard deviations of both components of horizontal wind are generally within 1 m s^{-1} over the lower 2000 m, and correlations of mean diurnal cycle model and profiler winds are between 0.6 and 0.75 over the lower 1500 m.

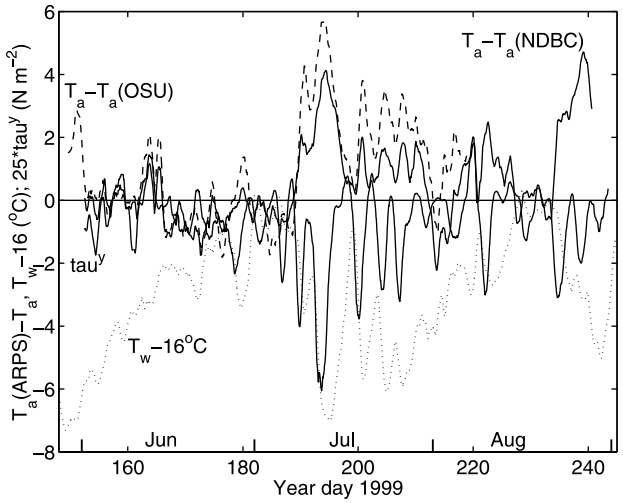

Figure 9. Alongshore wind stress at NDBC-46050 (thick solid line) and differences of model and NDBC-46050 (thin solid line) and model and OSU buoy (dashed line) surface air temperatures (°C) versus year day 1999. Wind stress time series has been multiplied by 25, so the effective units of stress are 0.04 N m^{-2}. The 2-m ocean temperature (°C, with a constant offset of −16) at the OSU buoy is also shown for comparison (dotted line). All time series have been smoothed with a 25-hour running mean.

The model qualitatively reproduces a double maximum in wind speed observed between 800 and 1500 m. The model overestimates the strength of the maximum observed 5 m s^{-1} southward flow at 200 m by 2.5 m s^{-1} and does not capture a persistent strong southward flow near 500 m during 0600–1500 UTC.

4. Discussion

4.1. Wind Forcing of the Coastal Ocean

[25] In many previous studies of wind-driven coastal upwelling off Oregon and elsewhere (and with some important exceptions [e.g., *Winant et al.*, 1988]), wind stress forcing has often been estimated from measurements from one or perhaps a few offshore buoys or coastal stations, and relatively little information has been available on the spatial variability of the wind field. The present results show that large spatial variations in mean and fluctuating wind stress occur systematically along the Oregon coast, with alongshore stress increasing by a factor of 3–4 from north to south along the coast. These results appear to be generally consistent with the large-scale pattern inferred from buoy and coastal observations by *Halliwell and Allen* [1987, Figures 3, 4, and 5], though the comparison is complicated by the relative sparseness of the buoys and coastal stations and by the uncertainty associated with estimating ocean stress from coastal stations.

[26] Near Cape Blanco the model and scatterometer results both indicate that mean and fluctuating alongshore stress change by nearly a factor of 2 over an alongshore distance of <100 km. Given the general similarity in lower atmospheric conditions and coastal orography, it can be inferred that this is an orographic intensification of the type previously observed at Point Arena along the northern California coast [*Winant et al.*, 1988; *Samelson*, 1992; *Samelson and Lentz*, 1994]. In situ observations of winds offshore and south of Cape Blanco were not available during summer 1999. Simultaneous shipboard and aircraft measurements during 23–26 August 1995 provide direct evidence that localized intensification of instantaneous wind fields does occur in this region (Figure 8). The model

results and scatterometer data reported above indicate that this intensification is a characteristic feature of the local wind field.

[27] The associated alongshore variations in alongshore wind stress will have important effects on the coastal ocean response. Observations have shown that the coastal upwelling jet tends to leave the coast near Cape Blanco [e.g., *Barth and Smith*, 1998; *Barth et al.*, 2000]. Previous studies have focused on the role of ocean bottom topography and coastline curvature in this process [e.g., *Dale and Barth*, 2001], but the results reported here suggest that enhanced local wind forcing could also control the circulation. The primary driving mechanism of upwelling circulation is wind-driven offshore Ekman transport, in which offshore surface currents are proportional to local alongshore wind stress. The model and scatterometer stress fields indicate that offshore Ekman transport is 3–4 times larger near Cape Blanco than along the northern Oregon coast and that coastal upwelling must be similarly intensified toward the south. This is consistent with the observed offshore displacement of the jet and with the observed presence of systematically colder ocean temperatures in this region. Also, the cross-shore variations in alongshore stress (i.e., the wind stress curl) that are evident in both the model and the scatterometer stress fields will presumably cause local Ekman transport divergences and convergences that may be dynamically significant.

[28] The mean diurnal cycle of stress at the buoys has an amplitude of roughly 0.02 N m^{-2}. If this mean diurnal stress were distributed over the upper 10 m of the water column, it would drive a linear response in horizontal currents of order 2 cm s^{-1}. This is similar to, though slightly smaller than, the amplitude of tidal currents observed by high-frequency radar during this period. In future work it may be possible to extract the stress-driven component of the observed diurnal surface currents and to distinguish it from the tidal component.

4.2. Upwelling and Coastal Air Temperature

[29] An important question in coastal environmental physics concerns the timescales of coupled ocean-atmosphere effects. A strong effect of wind-driven coastal ocean upwelling on surface air temperatures (SATs) can be inferred from the present atmospheric model results and buoy observations. Figure 9 shows the NDBC-46050 alongshore wind stress and shows the differences of modeled and observed SATs at both buoys during June–August 1999. The model-buoy SAT differences are often as large as 2–5°C and are correlated with strong southward wind stress events over most of the record. Lagged cross correlations between the wind stress and SAT difference time series in Figure 9 have (negative) maxima of −0.48 with 18-hour lag for SAT difference at the NDBC buoy and have (negative) maxima of −0.61 with 16 hour lag for SAT difference at the OSU buoy. (Note that the latter correlation is larger than the correlation of modeled and observed air temperature reported in Table 2). These correlations fall off rapidly for negative lags (temperature difference leading stress).

[30] These model-buoy SAT differences evidently arise because the SST boundary conditions used in the atmospheric model, which are derived from the NCEP Eta SST analyses, do not resolve the cold upwelled water near the coast. SAT differences are systematically greater between the model and the OSU buoy than between the model and NDBC-46050, consistent with the onshore decrease in SST associated with coastal upwelling. This onshore temperature decrease also appears in the buoy mean SATs (Tables 1 and 2). Analysis of 2-m ocean temperature (Figure 9) and model SST at the OSU buoy suggests that cold SATs develop first from cold SSTs inshore of the buoy and then spread offshore much more rapidly than the cold upwelled water itself, as the SAT difference and the model-buoy ocean temperature difference have a maximum cross correlation of 0.91, but with ocean temperature difference lagging SAT difference by 7 hours.

[31] We infer from this analysis and from the results in Figure 9 that coastal upwelling modifies coastal SAT by 1–5°C on time-scales of 12–24 hours. This implies that certain coastal atmospheric prediction problems, for example, forecasting coastal stratus, will evidently require a coupled ocean-atmosphere model.

[32] **Acknowledgments.** This research was supported by the National Oceanographic Partnership Program, Office of Naval Research (ONR) grant N00014-98-1-0787, by ONR grant N00014-98-1-0813, Code 322OM, and by National Aeronautics and Space Administration grant NAS5-32965 for funding of Ocean Vector Winds Science Team activities. The collection and analysis of shipboard data from August 1995 were supported by National Science Foundation grants OCE-9314370 and OCE-9730639. We are grateful to R. Kelly and G. Vali for generously making available the aircraft data from August 1995 and to J. S. Allen for comments on the manuscript.

References

Allen, J. S., Models of wind-driven currents on the continental shelf, *Ann. Rev. Fluid Mech.*, *12*, 389–433, 1980.

Barth, J., and R. L. Smith, Separation of a coastal upwelling jet at Cape Blanco, Oregon, USA, in *Benguela Dynamics: Impacts of Variability on Shelf-Sea Environments and their Living Resources*, edited by S. Pillar et al., *S. Afr. J. Mar. Sci.*, *19*, 5–14, 1998.

Barth, J., S. Pierce, and R. Smith, A separating coastal upwelling jet at Cape Blanco, Oregon, and its connection to the California Current System, *Deep Sea Res., Part II*, *47*, 783–810, 2000.

Beardsley, R., C. Dorman, C. Friehe, L. Rosenfeld, and C. Winant, Local atmospheric forcing during the Coastal Ocean Dynamics Experiments 1 and 2, 1, A description of the marine boundary layer and atmospheric conditions over a northern California upwelling region, *J. Geophys. Res.*, *92*, 1467–1488, 1987.

Bielli, S., P. Barbour, R. Samelson, E. Skyllingstad, and J. Wilczak, The diurnal cycle along the Oregon coast during summertime, *Mon. Weather Rev.*, *130*, 992–1008, 2002.

Black, T. L., The new NMC mesoscale eta model: Description and forecast examples, *Weather Forecast.*, *9*, 265–278, 1994.

Burk, S., and W. Thompson, The summertime low-level jet and marine boundary layer structure along the California coast, *Mon. Weather Rev.*, *124*, 668–686, 1996.

Dale, A., and J. Barth, The hydraulics of an evolving upwelling jet flowing around a cape, *J. Phys. Oceanogr.*, *31*, 226–243, 2001.

Freilich, M., and R. Dunbar, The accuracy of the NSCAT-1 vector winds: Comparisons with National Data Buoy Center buoys, *J. Geophys. Res.*, *104*, 11,231–11,246, 1999.

Halliwell, G., Jr., and J. S. Allen, The large-scale coastal wind field along the west coast of North America, 1981–1982, *J. Geophys. Res.*, *92*, 1861–1884, 1987.

Large, W., and S. Pond, Open ocean momentum flux measurements in moderate to strong winds, *J. Phys. Oceanogr.*, *11*, 324–336, 1981.

Naderi, F., M. Freilich, and D. Long, Spaceborne radar measurement of wind velocity over the ocean — An overview of the NSCAT scatterometer system, *Proc. IEEE*, *97*, 850–866, 1991.

Oke, P. R., J. S. Allen, R. Miller, G. D. Egbert, and P. M. Kosro, Assimilation of surface velocity data into a primitive equation coastal ocean model, *J. Geophys. Res.*, 10.1029/2000JC000511, in press, 2002.

Samelson, R., Supercritical marine-layer flow along a smoothly varying coastline, *J. Atmos. Sci.*, *49*, 1571–1584, 1992.

Samelson, R., and S. Lentz, The horizontal momentum balance in the marine atmospheric boundary layer during CODE-2, *J. Atmos. Sci.*, *51*, 3745–3757, 1994.

Winant, C., R. Beardsley, C. Dorman, and C. Friehe, The marine layer off northern California: An example of supercritical channel flow, *J. Atmos. Sci.*, *45*, 3588–3605, 1988.

Xue, M., K. Droegemeier, V. Wong, A. Shapiro, and K. Brewster, ARPS Version 4.0 User's Guide, 380 pp., Cent. for Anal. and Predict. of Storms, Univ. of Okla., Norman, Okla., 1995.

P. Barbour, J. Barth, S. Bielli, T. Boyd, D. Chelton, P. Kosro, M. Levine, R. Samelson, and E. Skyllingstad, College of Oceanic and Atmospheric Sciences, 104 Ocean Administration Building, Oregon State University, Corvallis, OR 97331–5503, USA. (barboup@engr.orst.edu; barth@coas.oregonstate.edu; soline@atmos.washington.edu; tboyd@coas.oregonstate.edu; chelton@coas.oregonstate.edu; mkosro@coas.oregonstate.edu; Levine@coas.oregonstate.edu; rsamelson@coas.oregonstate.edu; skylling@coas.oregonstate.edu)

J. Wilczak, Environmental Technology Laboratory, NOAA, 325 Broadway, Boulder, CO 80304, USA. (James.W.Wilczak@noaa.gov)